

## FE ANALYSIS ON THE FORMATION OF PLASTIC INSTABILITIES IN DYNAMICALLY EXPANDED COPPER RINGS

C. Vela<sup>1)</sup>, J.A. Rodríguez-Martínez<sup>1)</sup>, A. Rusinek<sup>2)</sup>

<sup>1)</sup> **University Carlos III of Madrid**  
**Department of Continuum Mechanics and Structural Analysis**

Avda. de la Universidad 30, 28911 Leganés, Madrid, Spain

<sup>2)</sup> **National Engineering School of Metz (ENIM)**  
**Laboratory of Mechanics, Biomechanics, Polymers and Structures (LaBPS)**

1 route d’Ars Laquenexy, 57078 Metz Cedex 3, France  
e-mail: rusinek@enim.fr

In this work the influence of the constitutive description in numerical simulations of the radial expansion of annealed **OFHC** copper rings has been studied. For that task, three physical-based constitutive models are implemented into the **FE** code ABAQUS/Explicit and applied to define the thermo-viscoplastic behaviour of the material in the simulations. These are those due to RUSINEK *et al.* [A. RUSINEK, J. A. RODRÍGUEZ-MARTÍNEZ, A. ARIAS, *A thermo-viscoplastic constitutive model for FCC metals with application to OFHC copper*, Int. J. Mech. Sci., **52**, 120–135, 2010], NEMAT-NASSER and LI [S. NEMAT-NASSER, Y. LI, *Flow stress of FCC polycrystals with application to OFHC Copper*, Acta Mater., **46**, 565–577, 1998] and VOYIADJIS and ALMASRI [G. Z. VOYIADJIS, A. H. ALMASRI, *A physically based constitutive model for fcc metals with applications to dynamic hardness*, Mech. Mater., **40**, 549–563, 2008]. The attention is primarily focussed on analyzing the influence of the material description on the strain localization process. Notable differences are observed in the response of the specimen under loading depending on the constitutive relation used. The numerical study indicated that the constitutive model controls the flow localization, defines the strain of instability and determines the number of necks formed. The causes which reside behind such decisive role played by the constitutive relation are investigated. It has been found that the rate sensitivity definition governs the models’ predictions for the strain localization process.

**Key words:** annealed OFHC copper, Fragmentation, Ring expansion, Constitutive description, Numerical simulation.

### 1. INTRODUCTION

Plastic instabilities play a prominent role in the deformation and failure of engineering materials subjected to dynamic loading [1–3]. Susceptibility of metals for instabilities formation determines their suitability for absorbing energy under dynamic solicitations. Understanding formation and propagation of instabilities in metals offers significant steps towards optimizing material’s behaviour

at high strain-rates [4–9]. Strain localization has gathered the efforts of many researchers [8–9, 10–16]. The seminal works of HUTCHINSON and NEALE [17], GHOSH [18] and FRESSENGEAS and MOLINARI [19–20] among others analysed the mechanisms responsible for plastic localization and instabilities progression.

Among the experimental arrangements applied to approach the localization problem under high loading rates, the ring expansion test has raised the interest of many investigators [21–26]. The main advantage of this test is that disturbances resulting from wave propagation are eliminated due to the symmetry of the problem (*under ideal boundary conditions and complete homogeneity of the material*) [23, 27–28] and the material ductility may be properly evaluated.

The test consists of loading a ring of radius  $R$  at a roughly constant velocity  $V_0$  within the range  $10 \text{ m/s} \leq V_0 \leq 300 \text{ m/s}$  [25–26]. The dynamic loading uses to be procured by a magnetic field or by the use of explosives. Among the previous testing techniques, the former displays an improved capacity for controlling the applied velocity. In any case, the mean strain rate  $\dot{\epsilon}(t)$  applied to the material during the test is defined by Eq. (1.1).

$$(1.1) \quad \dot{\epsilon}(t) = \frac{V_0}{R(t)},$$

where  $R(t)$  is the specimen radius as a function of time.

Large strains and strain rates that take place during the expansion of the ring lead to the formation of plastic instabilities inducing posterior fragmentation of the sample, Fig. 1.

Unfortunately, such kind of highly instrumented test is complicated to perform and requires of specific facilities. In order to avoid the complications arising from experimentation, recently the localization problem in expanded rings has attempted to be analytically described in the seminal works of MERCIER and MOLINARI [27] and ZHOU *et al.* [8]. In these publications a perturbation analysis is conducted in order to investigate the mechanisms which reside behind plastic localization. For this kind of analytical studies, due to complications in the mathematical formulation of the problem, the definition of the homogeneous material behaviour uses to be given by a simplified power-type equation [8, 27]. The accurate definition of the material behaviour is subordinated to a fast derivation of the problem solution. If *advanced* constitutive descriptions want to be used for defining the macroscopic behaviour of the material, numerical methods are a suitable alternative [28].

The term *advanced* uses to be tied to the physical-based constitutive models. They account for physical aspects of the material deformation behaviour. Most of them are founded on the theory of thermodynamics and kinetics of slip developed by KOCKS *et al.* [29]. Some examples are those models proposed in [30–36]. They allow for an accurate definition of the material behaviour un-

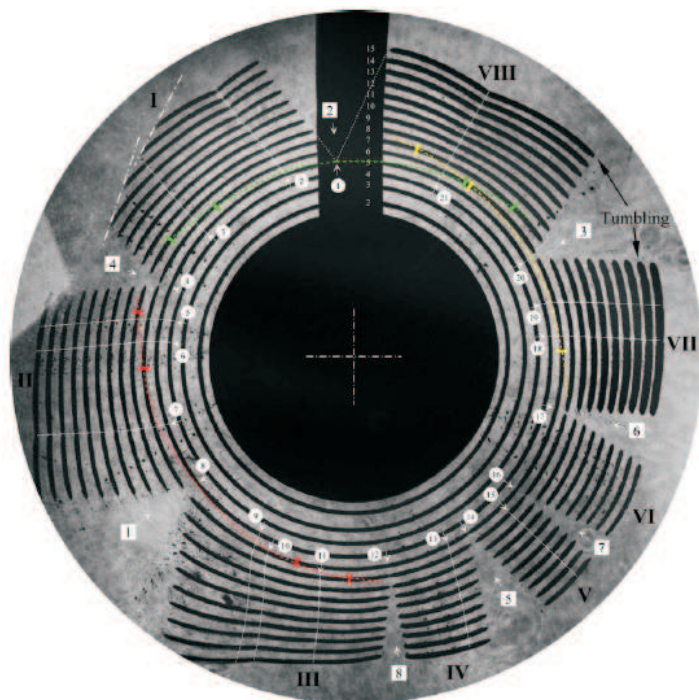


FIG. 1. Composite image for an Al 6061-O ring expanding test. Dimensions of the ring: 15.5 mm mean radius, 0.5 mm thick and 1 mm long. Applied velocity  $V_0 \approx 125$  m/s. The frame numbers are identified along the current lead on the top. The necks are identified at the location of their appearance by the numbers inside circles, numbering them counterclockwise. The fracture locations are identified by the numbers inside squares, numbering them in the time sequence of their appearance [25].

der wide a range of loading conditions. Due to their flexibility, physical-based models have an increasing interest for engineering applications like high speed machining, perforation [37], blast loading or crash-tests. In such processes, the material work-piece is subjected to wide ranges of strain rate and temperature as well as large deformation.

In this work the influence of constitutive description in numerical simulations of the radial expansion of annealed **OFHC** copper rings has been studied. For that task, three physical-based constitutive relations with proven efficiency for modelling this material have been implemented into the **FE** code ABAQUS/Explicit and applied in the simulations. These are those due to RUSINEK *et al.* [38], NEMAT-NASSER and LI [31] and VOYIADJIS and ALMASRI [36]. The main reasons that have led us to choose these constitutive descriptions are the rigor of their formulation (*all of them are based on the additive decomposition of the equivalent stress as it will be shown later in this paper*) and the relevance they have raised within the framework of metallic alloys modeling.

The numerical analysis revealed that the process of strain localization occurring in the sample during loading is strongly influenced by the material modelling. A systematic evaluation of the constitutive relations is performed to identify the causes behind this behaviour. It has been found that the rate sensitivity definition determines the models' predictions for instabilities formation.

## 2. CONSTITUTIVE MODELING OF THE ANNEALED OFHC COPPER

Copper is widely used in several industrial fields, typical applications of this metal include electrical and electronic applications, piping for water supplies, heat exchangers, manufacture of semiconductors and superconductor components and manufacture of high vacuum devices such as particle accelerators. Thus, polycrystalline **OFHC** copper is a typical **FCC** metal that has been widely used to explore the dependence of the flow stress on strain, strain rate and temperature [39–40]. Thus, it is clear the aroused interest by the processes of strain localization and fragmentation which occur in this material during dynamic solicitations.

Next, the constitutive descriptions applied for modelling the thermo-viscoplastic behaviour of this material in the simulations are briefly described.

### 2.1. The Extended Modified Rusinek–Klepaczko model to viscous drag effects

The **Extended Modified Rusinek–Klepaczko (EMRK)** [38] constitutive relation is based on the additive decomposition of the equivalent Huber–Mises stress  $\bar{\sigma}$  [30, 33, 35, 41–43], Eq. (2.1).

$$(2.1) \quad \bar{\sigma}(\bar{\varepsilon}^p, \dot{\bar{\varepsilon}}^p, T) = \frac{E(T)}{E_0} \cdot [\bar{\sigma}_\mu + \bar{\sigma}^*(\bar{\varepsilon}^p, \dot{\bar{\varepsilon}}^p, T)] + \bar{\sigma}_{vs}(\dot{\bar{\varepsilon}}^p),$$

where each term of the previous expression, Eq. (2.1), is defined below.

The multiplicative factor  $E(T)/E_0$  defines the Young's modulus evolution with temperature [44], Eq. (2.2).

$$(2.2) \quad E(T) = E_0 \left\{ 1 - \frac{T}{T_m} \exp \left[ \theta^* \left( 1 - \frac{T_m}{T} \right) \right] \right\}, \quad T > 0,$$

where  $E_0$ ,  $T_m$ , and  $\theta^*$  denote respectively the Young's modulus at  $T = 0$  K, the melting temperature and the characteristic homologous temperature. This expression allows for defining the material thermal softening depending on the crystal lattice [45]. In the case of **FCC** metals like copper  $\theta^* \approx 0.9$  as discussed in [38].

According to the considerations for **FCC** metals reported by several authors [30, 34, 46] the athermal stress  $\bar{\sigma}_\mu$  is defined independent of plastic strain. In agreement with [36] this stress component reads as follows, Eq. (2.3).

$$(2.3) \quad \bar{\sigma}_\mu = Y,$$

where  $Y$  is the flow stress at  $\bar{\varepsilon}^p = 0$ .

The thermal stress  $\bar{\sigma}^*(\bar{\varepsilon}^p, \dot{\bar{\varepsilon}}^p, T)$  describes macroscopically the rate controlling deformation mechanism from thermal activation. Based on the theory of thermodynamics and kinetics of slip [29], RUSINEK *et al.* [38] derived the following expression, Eq. (2.4).

$$(2.4) \quad \bar{\sigma}^*(\bar{\varepsilon}^p, \dot{\bar{\varepsilon}}^p, T) = B(\dot{\bar{\varepsilon}}^p, T) \cdot (\bar{\varepsilon}^p)^{n(\dot{\bar{\varepsilon}}^p, T)} \cdot \left\langle 1 - \xi_1 \left( \frac{T}{T_m} \right) \log \left( \frac{\dot{\varepsilon}_{\max}}{\dot{\bar{\varepsilon}}^p} \right) \right\rangle^{1/\xi_2},$$

where  $\xi_1$  and  $\xi_2$  are material constants describing temperature and rate sensitivities of the material,  $T_m$  is the melting temperature and  $\dot{\varepsilon}_{\max}$  defines the maximum rate level for application of the model.

The explicit formulations describing the modulus of plasticity  $B(\dot{\bar{\varepsilon}}^p, T)$  and the strain hardening exponent  $n(\dot{\bar{\varepsilon}}^p, T)$  are given by Eqs. (2.5)–(2.6).

$$(2.5) \quad B(\dot{\bar{\varepsilon}}^p, T) = B_0 \left( \left( \frac{T}{T_m} \right) \log \left( \frac{\dot{\varepsilon}_{\max}}{\dot{\bar{\varepsilon}}^p} \right) \right)^{-\nu}; \quad T > 0,$$

$$(2.6) \quad n(\dot{\bar{\varepsilon}}^p, T) = n_0 \left\langle 1 - D_2 \left( \frac{T}{T_m} \right) \log \left( \frac{\dot{\bar{\varepsilon}}^p}{\dot{\varepsilon}_{\min}} \right) \right\rangle,$$

where  $B_0$  is a material constant,  $\nu$  is tied to the material temperature sensitivity,  $n_0$  is the strain hardening exponent at  $T = 0$  K,  $D_2$  is a material constant and  $\dot{\varepsilon}_{\min}$  defines the minimum rate level for application of the model. The McCauley operator is defined as follows  $\langle \bullet \rangle = \bullet$  if  $\langle \bullet \rangle \geq 0$  or  $\langle \bullet \rangle = 0$  if  $\langle \bullet \rangle \leq 0$ . It has to be noted that previous expressions are dependent on strain rate and temperature. This feature, which is consistent with experimental evidences reported for most metals [47–48], makes the **EMRK** model appropriate to describe the formation of plastic instabilities in metallic alloys subjected to dynamic solicitations.

The viscous drag component  $\bar{\sigma}_{vs}(\dot{\bar{\varepsilon}}^p)$  provides a phenomenological description of the flow stress augment at high strain rates taking place in many metals due to the phonon drag effects in dislocation generation. The formulation used comes from the investigations due to KAPOOR and NEMAT-NASSER [49]. Based on theoretical considerations and supported by experimental evidences for a certain number of metals they proposed the following relation, Eq. (2.7).

$$(2.7) \quad \bar{\sigma}_{vs}(\dot{\bar{\varepsilon}}^p) = \chi \cdot [1 - \exp(-\alpha \cdot \dot{\bar{\varepsilon}}^p)],$$

where  $\chi$  is a material constant, and  $\alpha$  represents an effective damping coefficient affecting the dislocations' motion [50–51].

The material constants corresponding to annealed **OFHC** copper are listed in Table 1. They were obtained via a systematic procedure for calibration of the model. This procedure ensures the uniqueness of their values [38].

**Table 1. Material constants for annealed OFHC copper for the EMRK model [38].**

$Y$ [MPa]	$B_0$ [MPa]	$\nu$ [-]	$n_0$ [-]	$D_2$ [-]	$\xi_2$ [-]	$\xi_1$ [-]	$\chi$ [MPa]	$\alpha$ [s <sup>-1</sup> ]	$T_m$ [K]	$\dot{\epsilon}_{\min}$ [s <sup>-1</sup> ]	$\dot{\epsilon}_{\max}$ [s <sup>-1</sup> ]	$\theta^*$ [-]
40	560.28	0.30447	0.492	0.0553	0.0131	0.0011932	249	0.0000122	1340	10 <sup>-5</sup>	10 <sup>7</sup>	0.9

Next, the constitutive description proposed by NEMAT–NASSER and LI (NNL) [31] is introduced.

### 2.2. The Nemat–Nasser – Li model

In the same manner as the **EMRK** constitutive description, the **NNL** model decomposes the equivalent stress  $\bar{\sigma}$  into thermal  $\bar{\sigma}^*(\bar{\epsilon}^p, \dot{\bar{\epsilon}}^p, T)$  and athermal  $\bar{\sigma}_\mu(\bar{\epsilon}^p)$  components, Eq. (2.8),

$$(2.8) \quad \bar{\sigma}(\bar{\epsilon}^p, \dot{\bar{\epsilon}}^p, T) = \bar{\sigma}_\mu(\bar{\epsilon}^p) + \bar{\sigma}^*(\bar{\epsilon}^p, \dot{\bar{\epsilon}}^p, T).$$

The athermal stress term is defined as a function of the equivalent plastic strain, Eq. (2.9).

$$(2.9) \quad \bar{\sigma}_\mu(\bar{\epsilon}^p) = \sigma_a^0 \cdot (\bar{\epsilon}^p)^{n_1},$$

where  $\sigma_a^0$  and  $n_1$  (which, on contrary to the **EMRK** model, are assumed constant) are material parameters describing the flow stress level and the strain hardening of the material.

The thermal stress is defined by Eq. (2.10). It depends on plastic strain, strain rate and temperature.

$$(2.10) \quad \bar{\sigma}^*(\bar{\epsilon}^p, \dot{\bar{\epsilon}}^p, T) = \sigma^0 \cdot \left( 1 - \left( -\frac{k \cdot T}{G_0} \cdot \left( \ln \left( \frac{\dot{\bar{\epsilon}}^p}{\dot{\epsilon}_0} \right) + \ln (1 + a(T) \cdot (\bar{\epsilon}^p)^{n_0}) \right) \right)^{1/q} \right)^{1/p} \cdot (1 + a(T) \cdot (\bar{\epsilon}^p)^{n_0}),$$

where  $\sigma^0$  is a material constant,  $k$  is the Boltzmann's constant,  $G_0$  is the reference Gibbs free energy at  $T = 0$  K,  $\dot{\epsilon}_0$  is the reference strain rate,  $n_0$  is a material

parameter defining strain hardening (*assumed constant*) and  $p$  and  $q$  are parameters describing the profile of the short range energy barrier to the motion of dislocations. Moreover,  $a(T)$  is an empirical function depending on temperature and tied to the average dislocation spacing (*free path*), Eq. (2.11).

$$(2.11) \quad a(T) = a_0 \left( 1 - \left( \frac{T}{T_m} \right)^{n_2} \right),$$

where  $a_0$  and  $n_2$  are material constants.

The material constants corresponding to annealed **OFHC** copper are listed in Table 2.

**Table 2. Material constants for annealed OFHC copper for the NNL model [31].**

$p$	$q$	$k/G_0$	$\dot{\varepsilon}_0$	$a_0$	$\sigma^0$	$\sigma_a^0$	$n_0$	$n_1$	$n_2$
[–]	[–]	[K <sup>-1</sup> ]	[s <sup>-1</sup> ]	[–]	[MPa]	[MPa]	[–]	[–]	[–]
2/3	2	0.000049	2*10 <sup>10</sup>	20	46	220	0.5	0.3	2

In the following section of the manuscript, the constitutive relation due to VOYIADJIS and ALMASRI (**VA**) [36] is introduced.

### 2.3. The Voyiadjis–Almasri model

VOYIADJIS and ALMASRI [36] derived a physically-based model founded on the concept of thermal activation analysis. In the same manner as the **EMRK** and **NNL** models, the **VA** splits into two parts the equivalent stress  $\bar{\sigma}$ . This is the addition of the equivalent thermal stress  $\bar{\sigma}^*(\bar{\varepsilon}^p, \dot{\bar{\varepsilon}}^p, T)$  and the equivalent athermal stress  $\bar{\sigma}_\mu$ , Eq. (2.12),

$$(2.12) \quad \bar{\sigma}(\bar{\varepsilon}^p, \dot{\bar{\varepsilon}}^p, T) = \bar{\sigma}_\mu + \bar{\sigma}^*(\bar{\varepsilon}^p, \dot{\bar{\varepsilon}}^p, T).$$

As the **EMRK** formulation, Eq. (2.1), the **VA** model defines the athermal stress independent of plastic strain, Eq. (2.13).

$$(2.13) \quad \bar{\sigma}_\mu = Y_a,$$

where  $Y_a$  is a material constant describing the stress component temperature and rate independent.

The thermal stress is defined as a function of plastic strain Eq. (2.14),

$$(2.14) \quad \bar{\sigma}^*(\bar{\varepsilon}^p, \dot{\bar{\varepsilon}}^p, T) = (B_0 \cdot \bar{\varepsilon}_p^n) \cdot \left( 1 + B_1 \cdot T \cdot (\dot{\bar{\varepsilon}}_p)^{1/m} - B_2 \cdot T \cdot \exp \left( A \left( 1 - \frac{T}{T_t} \right) \right) \right).$$

In the previous expression  $B$  and  $n$  denote the strain hardening modulus and the strain hardening exponent respectively (*which, on contrary to the EMRK model, are assumed constant*). Moreover  $B_1$  and  $B_2$  are material constants tied to mobile dislocation density evolution and to thermodynamic material parameters [36],  $m$  defines the strain rate sensitivity and  $A$  is a material constant.

The material constants corresponding to annealed **OFHC** copper are listed in Table 3.

**Table 3. Material constants for annealed OFHC copper for the VA model [36].**

$Y_a$ [MPa]	$B_0$ [MPa]	$n$ [-]	$B_1$ [K <sup>-1</sup> ]	$B_2$ [K <sup>-1</sup> ]	$m$ [-]	$A$ [-]	$T_t$ [K]
0	600	0.42	0.0000004	0.001	1.15	0.001	610

In the case of adiabatic conditions of deformation the constitutive relations previously presented are combined with the energy balance principle, Eq. (2.15). Such relation allows for an approximation of the thermal softening of the material via the adiabatic heating.

$$(2.15) \quad \Delta T(\bar{\varepsilon}^p, \bar{\sigma}) = \frac{\beta}{\rho C_p} \int_0^{\bar{\varepsilon}_{\max}^p} \bar{\sigma}(\bar{\varepsilon}^p, \dot{\bar{\varepsilon}}^p, T) d\bar{\varepsilon}^p,$$

where  $\beta$  is the Taylor-Quinney coefficient assumed as constant,  $\rho$  is the material density and  $C_p$  is the specific heat at constant pressure. Transition from isothermal to adiabatic conditions of deformation is assumed at  $\dot{\varepsilon} = 10 \text{ s}^{-1}$  in agreement with experimental observations reported for metallic materials in [52–53].

Conventional physical constants of annealed **OFHC** copper may be obtained from material handbooks, Table 4.

**Table 4. Physical constants for annealed OFHC copper.**

$E_0$ [GPa]	$C_p$ [Jkg <sup>-1</sup> K <sup>-1</sup> ]	$\beta$ [-]	$\rho$ [kgm <sup>-3</sup> ]
130	385	0.9	8960

In the following section of the document the analytical predictions of previous models are compared with experiments [31]. The definition they provide of the thermo-viscoplastic material behaviour is discussed.

### 3. APPLICATION OF EMRK, NNL AND VA MODELS TO ANNEALED OFHC COPPER

In Fig. 2 is depicted the comparison between analytical predictions of the models and experiments at room temperature for two values of strain rate,  $\dot{\epsilon} = 0.1 \text{ s}^{-1}$  and  $\dot{\epsilon} = 8000 \text{ s}^{-1}$  (*The former strain rate corresponding to isothermal conditions of deformation, the latter to adiabatic*). Satisfactory agreement is observed in, Fig. 2.

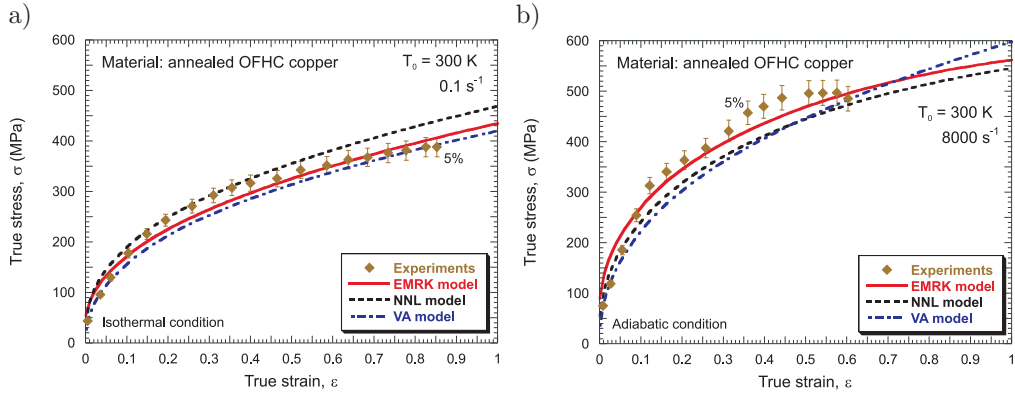


FIG. 2. Description of the flow stress evolution as a function of strain using **EMRK**, **NNL** and **VA** models and comparison with experiments at room temperature: a)  $0.1 \text{ s}^{-1}$ , b)  $8000 \text{ s}^{-1}$  [31].

However for strain rate levels between those analyzed in previous graphs,  $0.1 \text{ s}^{-1} < \dot{\epsilon} < 8000 \text{ s}^{-1}$ , the **VA** model provides predictions of material flow stress quite lower than those due to the **EMRK** and **NNL** formulations, Fig. 3.

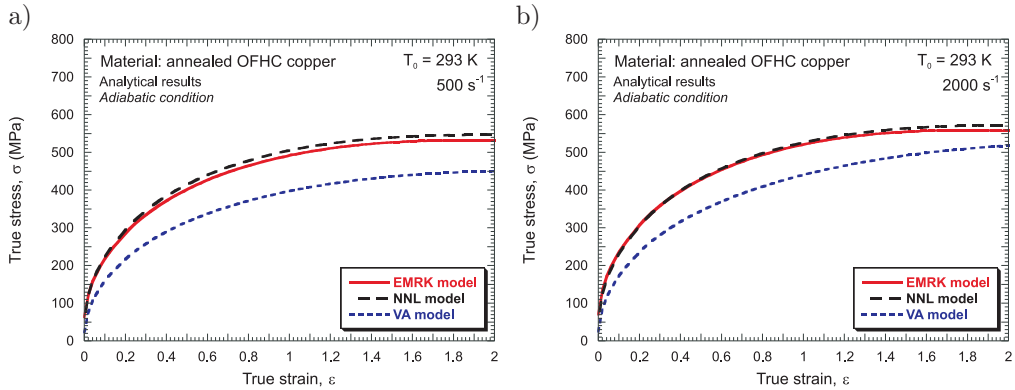


FIG. 3. Description of the flow stress evolution as a function of strain using **EMRK**, **NNL** and **VA** models at room temperature: a)  $500 \text{ s}^{-1}$ , b)  $2000 \text{ s}^{-1}$ .

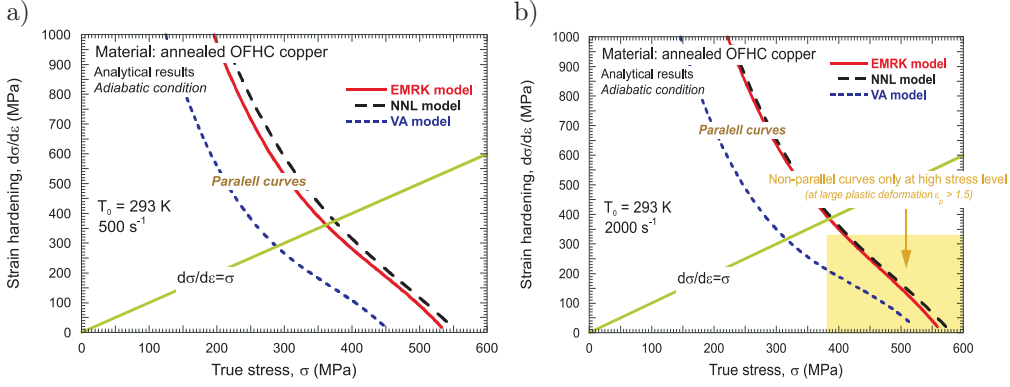


FIG. 4. Description of the strain hardening evolution as a function of stress using **EMRK**, **NNL** and **VA** models at room temperature: a)  $500 \text{ s}^{-1}$ , b)  $2000 \text{ s}^{-1}$ .

Nevertheless, it must be highlighted that the strain hardening definition provided by the three models is quite similar for the whole range of strain rates analyzed in this paper, Fig. 4.

The differences in the flow stress level mentioned above come from the rate sensitivity definition predicted by each constitutive relation, Fig. 5. Those differences are especially remarkable within the range of strain rates covered in the numerical simulations conducted in this work,  $100 \text{ s}^{-1} < \dot{\epsilon} < 10000 \text{ s}^{-1}$ , Fig. 5.

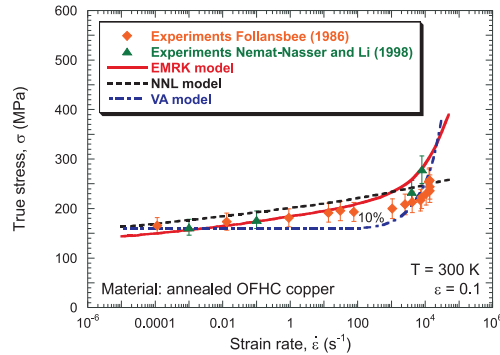


FIG. 5. Description of the flow stress evolution as a function of strain rate using **EMRK**, **NNL** and **VA** models and comparison with experiments at room temperature for  $\epsilon = 0.1$  [31, 54].

In Fig. 6 is illustrated the rate sensitivity predicted by the constitutive relations considered for two values of strain,  $\epsilon = 0.1$  and  $\epsilon = 0.5$ . The **NNL** model shows quite reduced rate sensitivity, lower than that provided by the **EMRK** formulation for the whole range of strain rates considered, Fig. 6. It has to be noted that for  $\dot{\epsilon} \leq 10 \text{ s}^{-1}$  the rate sensitivity shown by the **VA** model

is practically nil. Nevertheless, beyond that point the rate sensitivity exhibited by this model sharply increases and it quickly exceeds the **EMRK** and **NNL** predictions, Fig. 6.

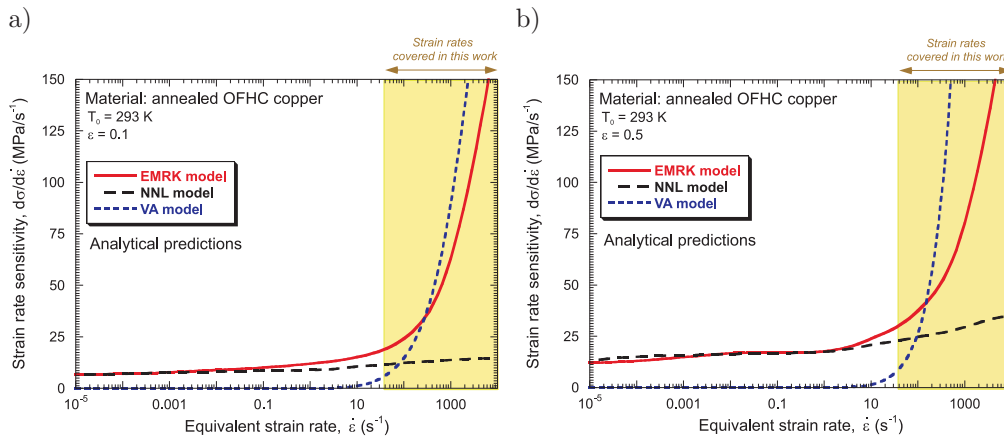


FIG. 6. Rate sensitivity predicted by the three models considered for different values of strain at room temperature: a)  $\epsilon = 0.1$ , b)  $\epsilon = 0.5$ .

In the following section of the manuscript, the numerical model built for simulation of the ring expansion problem is described.

#### 4. NUMERICAL MODEL AND VALIDATION

##### 4.1. Numerical model

The geometry and dimensions of the ring are based on a previous work [28], Fig. 7. The inner diameter of the ring is  $\phi = 30$  mm, with a thickness of

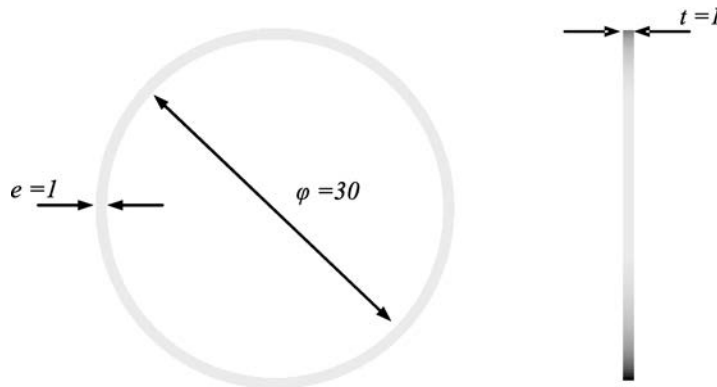


FIG. 7. Geometry and dimensions (mm) of the specimen used in the simulations [28].

$e = 1$  mm and a width of  $t = 1$  mm ( $1 \text{ mm}^2$  square cross section). The impact velocity is applied in the inner surface of the ring and remains constant during the whole loading process [28] leading to the strain rate decrease described by Eq. (1.1).

The mesh used is shown in Fig. 8. Three elements are placed along the thickness and width of the sample. The ring has been meshed using hexahedral elements whose aspect ratio is close to 1:1:1 ( $\approx 0.33 \times 0.33 \times 0.33 \text{ mm}^3$ ). This definition is in agreement with the considerations reported by ZUKAS and SCHEFFLER [55]. No geometrical or material imperfections were introduced in the model [56] since they could perturb the necking process [57–58].

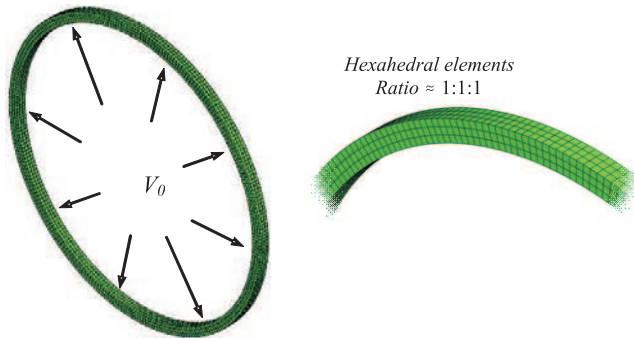


FIG. 8. Mesh configuration used in the numerical simulations. Symmetric mesh without any geometrical imperfection.

The boundary conditions applied to the simulations must guarantee the uniaxial tensile state in the specimen during loading.

It must be noticed that the strain of instability is intrinsically tied to the definition of the homogenous material behaviour (*constitutive description used to define the material behaviour*). Thus, in agreement with RUSINEK and ZAJARA [28], a constant critical failure strain,  $\bar{\epsilon}_f^p = 2.5$ , has been used in the simulations (*erosive failure criterion involving element deletion*). The condition that must be imposed to the failure strain is to be large enough to not disturb plastic localization and necking development. If such condition is fulfilled, the number of necks is not affected by the failure strain level. The numerical uncertainties through the integration process being enough to perturb the stress and deformation fields [28]. Then, wave reflections and interactions take place leading to strain localization in the absence of geometrical or material irregularities [60].

It has to be highlighted that considering a viscoplastic material model acts as a regularization method for solving mesh-dependent strain softening problems of plasticity [7]. Rate dependent plasticity introduces implicitly a length-scale

parameter into the boundary value problem diffusing the localization region [59]. It guarantees the well-posedness of the problem and the uniqueness of the numerical solution [60].

The three constitutive relations here analyzed have been implemented into ABAQUS/Explicit **FE** code via a **VUMAT** subroutine by means of the thermo-viscoplastic integration scheme for Huber-Misses plasticity proposed by ZAERA and FERNÁNDEZ-SÁEZ [61].

#### 4.2. Validation of the numerical model

Numerical simulations within the range of impact velocities  $5 \text{ m/s} \leq V_0 \leq 150 \text{ m/s}$  have been carried out. Stress – strain curves obtained from simulations are compared with analytical predictions of the constitutive relations. In the simulations, the measurement is conducted on an integration point belonging to an element out of the necking zone, Fig. 9. There, the flow stress can be considered homogeneous.

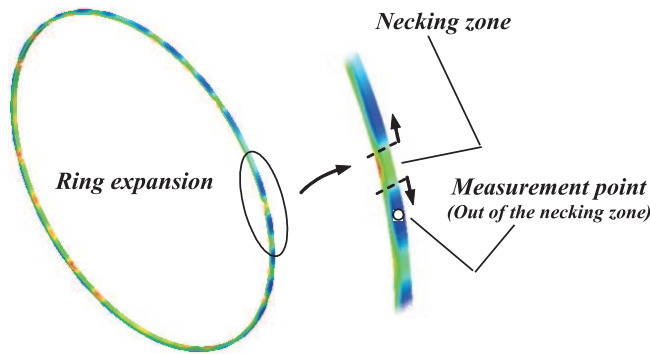


FIG. 9. Measurement point of strain-stress curves for validation of the model.

It has been already mentioned that the strain rate is not constant along the test. However, since the decrease of the strain rate during loading will be quite reduced, let us assume that a satisfactory comparison between analytical predictions and simulations can be conducted. The analytical predictions are obtained using the initial strain rate applied to the test. Perfect matching is observed between analytical predictions and simulation results (*for the EMRK model the decrease of the strain rate during the test is responsible for the small disagreement taking place at large deformation*), Fig. 10. This validates the numerical model developed and the implementation of the constitutive relations into the **FE** code.

In the following section of the manuscript the results obtained from the numerical simulations are discussed.

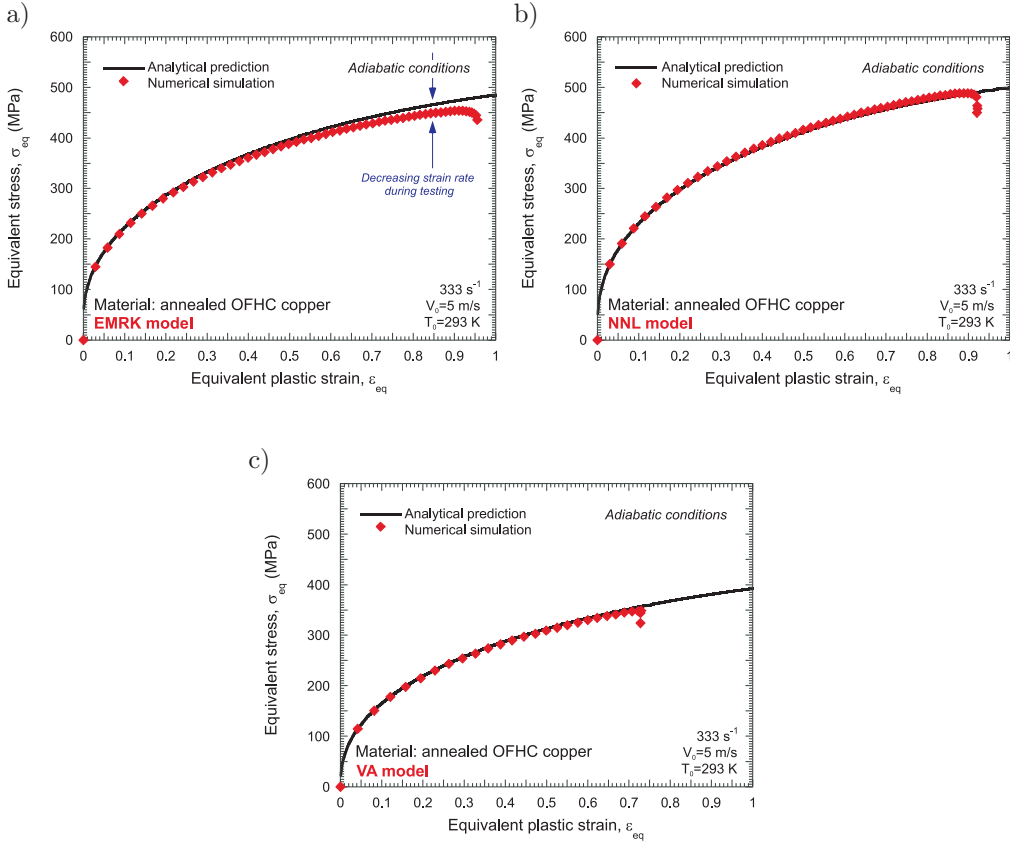


FIG. 10. Comparison between numerical results and analytical predictions for the three models considered at  $V_0 = 5 \text{ m/s}$ .

## 5. NUMERICAL RESULTS AND DISCUSSION

The first step is to analyze the evolution of the local plastic strain (*in the necking*) as a function of the global one (*theoretical deformation corresponding to homogeneous behaviour*) for all the constitutive descriptions and different impact velocities. The measurement of the local plastic strain is conducted as depicted in Fig. 11.

The calculation of the global deformation is carried out via Eq. (5.1).

$$(5.1) \quad \varepsilon_{\text{global}}(t) = \ln \left( \frac{R(t)}{R_0} \right),$$

where  $R_0$  is the initial radius of the sample and  $R(t)$  is the specimen radius as a function of time obtained from the simulations.

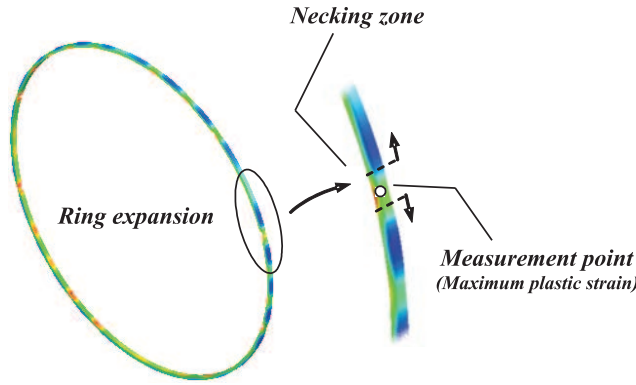


FIG. 11. Measurement point of local plastic strain.

By application of this procedure the following graphs are obtained, Fig. 12. Until necking takes place the local plastic strain agrees with the theoretical one. Once instability is formed, the local plastic strain drastically deviates from the global specimen deformation [62]. The bifurcation point (*strain of instability*) is highly dependent on impact velocity as well as on the constitutive model applied, Fig. 12.

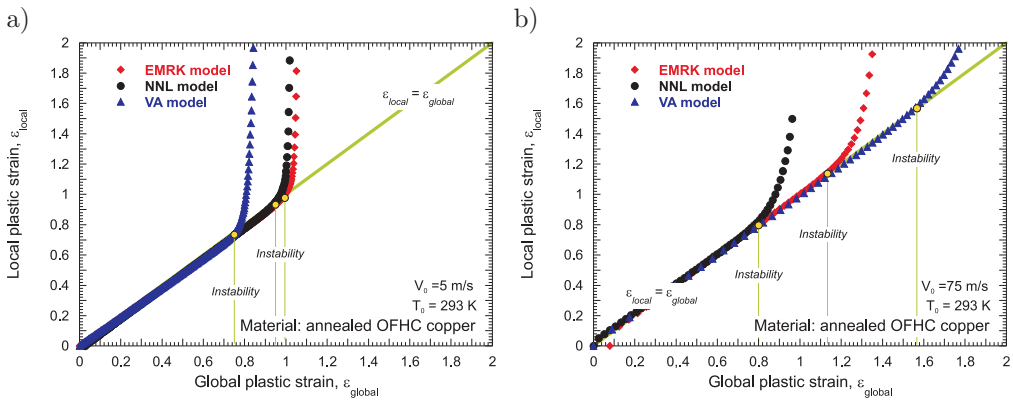


FIG. 12. Local plastic strain as a function of the global plastic strain for the three constitutive descriptions considered: a)  $V_0 = 5 \text{ m/s}$ , b)  $V_0 = 75 \text{ m/s}$ .

It can be observed that the strain of instability predicted by the **EMRK** model is larger than that predicted by the **NNL** model for both velocities checked, Fig. 12. Moreover, it is interesting to notice that in the case of  $V_0 = 5 \text{ m/s}$  the smallest strain of instability  $\epsilon$  corresponds to the **VA** constitutive description, however for  $V_0 = 75 \text{ m/s}$  it predicts the largest one, Fig. 12.

Such trends are confirmed analyzing the evolution of the local plastic strain rate in the necking as a function of the global plastic strain, Fig. 13. In such

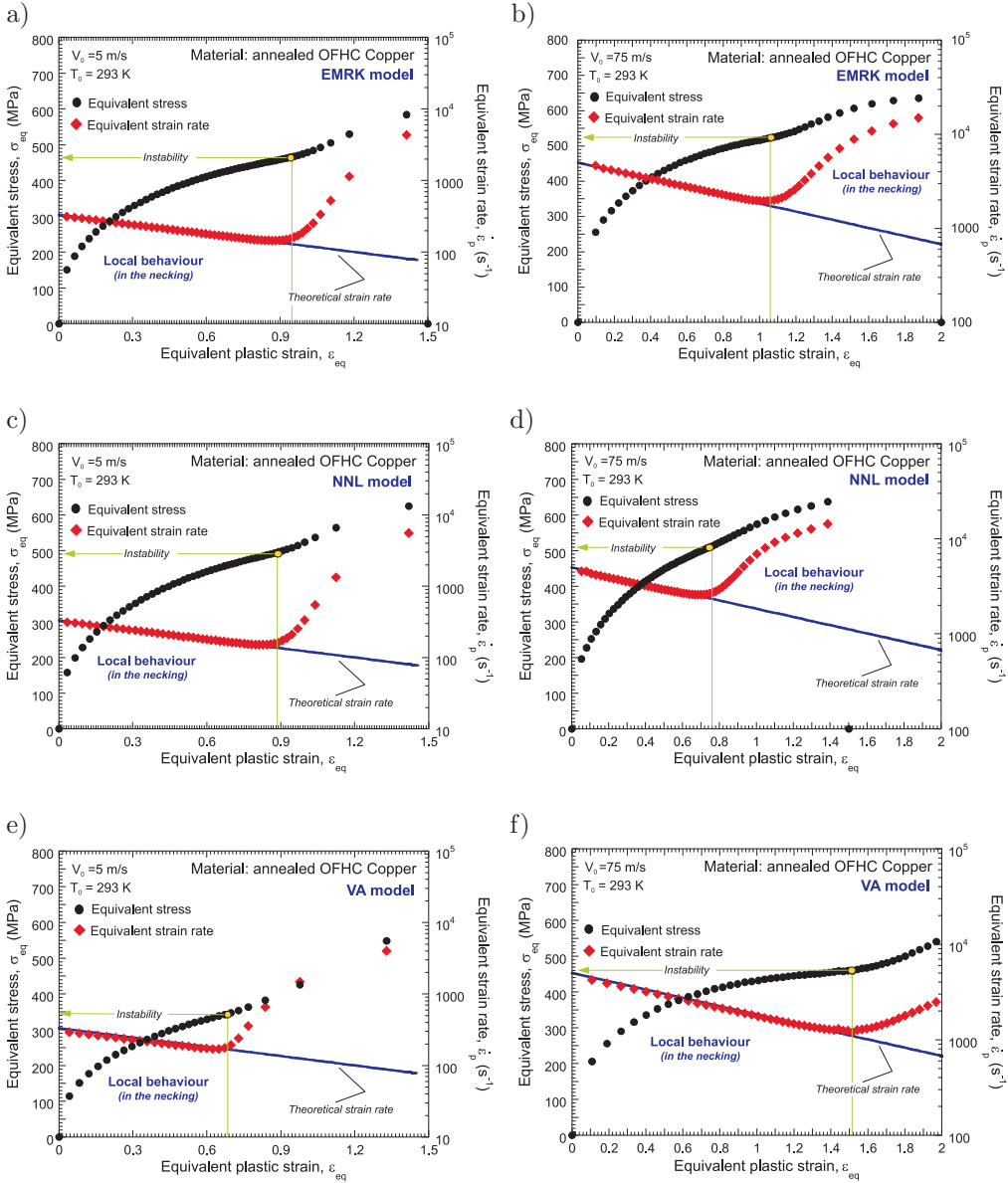


FIG. 13. Local strain rate and local flow stress as a function of the global plastic strain for the three constitutive descriptions considered and two impact velocities:  
a), c), e)  $V_0 = 5$  m/s. b), d), f)  $V_0 = 75$  m/s.

a case the strain of instability is determined by the bifurcation point of the local strain rate from the theoretical one, Eq. (1.1), Fig. 13. Necking formation involves a sharp augment of the local strain rate and flow stress.

In order to go further in this investigation let us depict the evolution of the strain of instability and the time of instability as a function of the impact velocity for the three models considered, Fig. 14. For the whole range of impact velocities, the strain of instability predicted by the **EMRK** model is larger than that determined by the **NNL** formulation. The difference between the predictions of both models increases with the impact velocity applied to the ring. Moreover, the **VA** constitutive description shows the lowest strain of instability until  $V_0 = 10$  m/s, Fig. 14. Then, it exceeds the predictions of **EMRK** and **NNL** models and the strain of instability shown by the **VA** constitutive relation becomes the largest one. The range of impact velocities  $V_0 < 10$  m/s corresponds to initial strain rate of the test  $\dot{\epsilon} \leq 650$  s $^{-1}$  (*the strain rate applied to the material will decrease during loading from this value*). It has to be noted that within that range of strain rates the rate sensitivity predicted by the **VA** model is the lowest one, Fig. 5. The range of impact velocities  $V_0 > 10$  m/s corresponds to initial strain rate of the test  $\dot{\epsilon} \geq 650$  s $^{-1}$ . It has to be noted that within that range of strain rates the rate sensitivity predicted by the **VA** model becomes the largest one, Fig. 5. It seems to be clear that rate sensitivity and strain of instability are closely related.

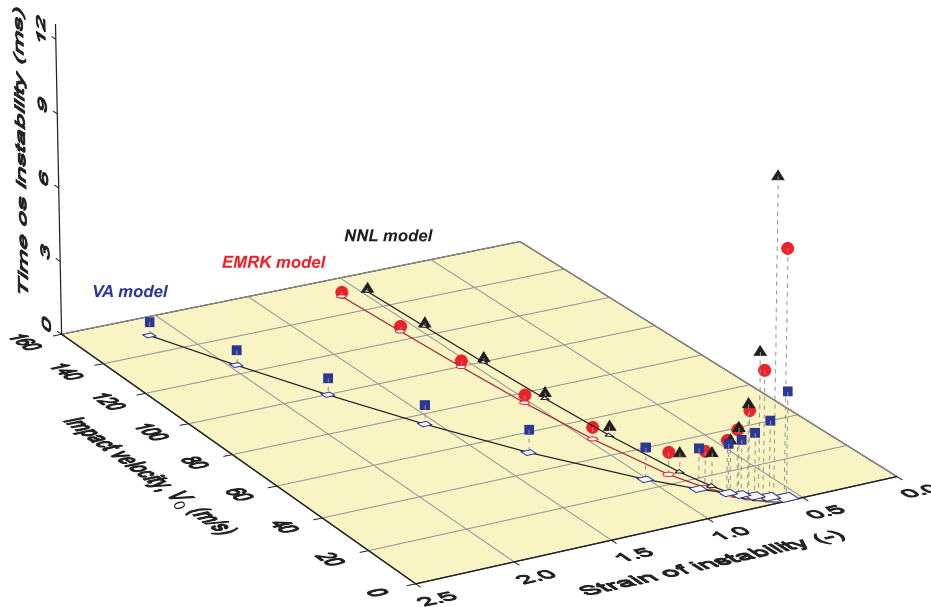


FIG. 14. Strain and time of instability as a function of impact velocity for the three constitutive descriptions considered.

The larger the rate sensitivity, the larger the strain of instability (*It has to be taken into account that the strain hardening predictions of all the models are*

very similar, Fig. 4. Strain hardening is not responsible for the differences in the strain of instability shown in Fig. 14). This consideration explains the increasing strain of instability with impact velocity exhibited by the three constitutive relations, Fig. 14. Since all constitutive models show increasing rate sensitivity with strain rate augment (*within the range of impact velocities considered in this investigation*), the strain of instability is always increasing with impact velocity (*this trend is also enhanced by effect of inertia* [24]). Within the range of impact velocities into which the **VA** model shows the lowest rate sensitivity, it predicts the smallest time of instability. Opposite behaviour is observed within the range of impact velocities into which the **VA** formulation predicts the largest rate sensitivity, Fig. 14.

Moreover, it has been analyzed the number of necks taking place in the sample (*as previously discussed the number of necks is independent of the failure strain applied in the simulations if this is large enough to not disturb the strain localization process*), Fig. 15. Increasing impact velocity leads to increasing number of necks for all the models analyzed [27–28].

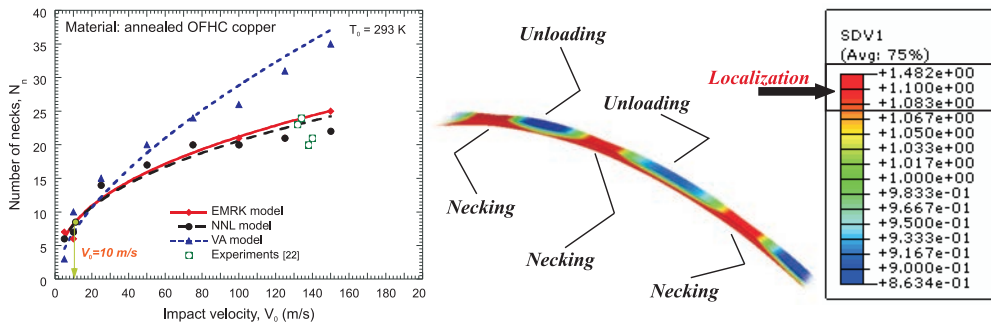


FIG. 15. Number of necks as a function of the impact velocity for the three constitutive descriptions considered and comparison with experiments [22]. Plastic strain contours of the ring during loading for determination of the number of necks.

It has to be highlighted that, within the range of impact velocities  $100 \text{ m/s} \leq V_0 \leq 150 \text{ m/s}$ , both **EMRK** and **NNL** constitutive models seem to provide satisfactory predictions of the number of necks in comparison with the experimental data reported by GRADY and BENSON [22], Fig. 15. However, the **VA** model predicts much larger number of necks than those observed in experiments. Such disagreement seems to be caused rate sensitivity definition that the **VA** model shows at high strain rates.

It is concluded that the rate sensitivity acts as a key variable for controlling the strain localization processes taking place in metals subjected to dynamic loading. If a constitutive description is applied for predicting the thermoviscoplastic response of a metallic alloy subjected to impact loading, it has

to provide a precise description of the material rate sensitivity. Otherwise the confidence on the results obtained from such analysis should be questioned. Accuracy in constitutive modelling of metals is a key point in numerical analyses of dynamic processes.

## 6. CONCLUDING AND REMARKS

This work presents a numerical analysis on the role played by the constitutive description on the strain localization process in the radial expansion of copper rings. For that task, three physical-based constitutive relations have been implemented into the **FE** code ABAQUS/Explicit and applied in the simulations. These are the **Extended Modified Rusinek–Klepaczko**, the **Nemat–Nasser–Li** and the **Voyiadjis–Almasri** constitutive descriptions. Numerical simulations within the range of impact velocities  $5 \text{ m/s} \leq V_0 \leq 150 \text{ m/s}$  have been carried out. The analysis revealed that the process of strain localization occurring in the sample during loading is strongly influenced by the material modelling. It has been found that the rate sensitivity definition determines the model predictions for instabilities formation. The application of numerical methods for solving dynamic initial-boundary value problems requires of constitutive descriptions providing a very accurate description of the material rate sensitivity within wide ranges of loading conditions.

## ACKNOWLEDGMENT

The researchers of the University Carlos III of Madrid are indebted to the Comunidad Autónoma de Madrid (Project CCG08-UC3M/MAT-4464) and to the Ministerio de Ciencia e Innovación de España (Project DPI/2008-06408) for the financial support received which allowed conducting part of this work.

## REFERENCES

1. R. P. PAPIRNO, J. F. MESCALL, A. M. HANSEN, *Beyond the Taylor test to fracture*, [in:] *Designing for extremes: Environment, loading, and structural behavior*, Proceedings of the Army Symposium on Solid Mechanics, pp. 367–385, Watertown, MA, September 1980. Army Materials and Mechanics Research Center.
2. H. COUQUE, *On the use of the symmetric Taylor test to evaluate dynamic ductile compression fracture properties of metals*, Proceedings of the 5th International Conference on Structures Under Shock and Impact, pp. 579–589, Computational Mechanics Inc, Billerica, MA, USA, 1998.
3. A. MOLINARI, C. MUSQUAR, G. SUTTER, *Adiabatic shear banding in high speed machining of Ti–6Al–4V: Experiments and modeling*, Int. J. Plasticity, **18**, 443–459, 2002.

4. M. K. DUSZEK, P. PERZYNA, *The localization of plastic deformation in thermoplastic solids*, Int. J. Solids and Struct., **27**, 1419–1443, 1991.
5. T. ŁODYGOWSKI, M. LENGNICK, P. PERZYNA, E. STEIN, *Viscoplastic numerical analysis of dynamic plastic strain localization for a ductile material*, Arch. Mech., 46, 4, 541–557, 1994.
6. P. PERZYNA, *Instability phenomena and adiabatic shear band localization in thermoplastic flow processes*, Acta Mechanica, **106**, 173–205, 1994.
7. A. GLEMA, T. ŁODYGOWSKI, P. PERZYNA, *Interaction of deformation waves and localization phenomena in inelastic solids*, Comput. Methods Appl. Mech. Engrg., **183**, 123–140, 2000.
8. F. ZHOU, J. F. MOLINARI, K. T. RAMESH, *An elasto-visco-plastic analysis of ductile expanding ring*, Int. J. Impact Eng., **33**, 880–891, 2006.
9. D. RITTEL, G. RAVICHANDRAN, A. VENKERT, *The mechanical response of pure iron at high strain rates under dominant shear*, Mat. Sci. Eng. A., **1–2**, 191–201, 2006.
10. H. C. MANN, *High-velocity tension-impact tests*, Proc. ASTM, **36**, 85, 1936.
11. J. R. KLEPACZKO, *Generalized conditions for stability in tension test*, Int. J. Mech. Sci., **10**, 297–313, 1968.
12. A. M. RAJENDRAN, I. M. FYFE, *Inertia effects on the ductile failure of thin rings*, Journal of Applied Mechanics, Transactions of the ASME, **49**, 31–36, 1982.
13. R. J. CLIFTON, J. DUFFY, K. A. HARTLEY, T. G. SHAWKI, *On the critical conditions for shear band formation at high strain rates*, Scripta Metall., **5**, 443–448, 1984;.
14. R. C. BATRA, C. H. KIM, *Effect of viscoplastic flow rules on the initiation and growth of shear bands at high strain rate*, J. Mech. Phys. Solids, **6**, 859–874, 1990.
15. J. R. KLEPACZKO, *Remarks on impact shearing*, J. Mech. Phys. Solids, **35**, 1028–1042, 1998.
16. Z. XUE, A. VAZIRI, J. W. HUTCHINSON, *Material aspects of dynamic neck retardation*, J. Mech. Phys. Solids, **56**, 93–113, 2008.
17. J. W. HUTCHINSON, K. W. NEALE, *Influence of strain rate sensitivity on necking under uniaxial tension*, Acta Metall., **25**, 839–846, 1977.
18. A. K. GHOSH, *Tensile instability and necking in materials with strain hardening and strain-rate hardening*, Acta Metall., **25**, 1413–1424, 1977.
19. C. FRESSENGEAS, A. MOLINARI, *Instability and localization of plastic flow in shear at high strain rates*, J. Mech. Phys. Solids, **2**, 185–211, 1987;.
20. C. FRESSENGEAS, A. MOLINARI, *The time development of Eulerian/Lagrangian perturbations to simple shear and its applications to shear banding*, J. Mech. Phys. Solids, **8**, 1735–1756, 1992.
21. F. L. NIORDSON, *A unit for testing materials at high strain rates*, Exp. Mech., **5**, 29–32, 1965.
22. D. E. GRADY, D. A. BENSON, *Fragmentation of metal rings by electromagnetic loading*, Exp. Mech., **12**, 393–400, 1983.

23. X. HU, G. S. DAEHN, *Effect of velocity on flow localization in tension*, Acta Mater., **44**, 1021–1033, 1996.
24. M. ALTYSNOVA, X. HU, G. S. DAEHN, *Increased ductility in high velocity electromagnetic ring expansion*, Metall. Trans. A, **27**, 1837–1844, 1996.
25. H. ZHANG, K. RAVI-CHANDAR, *On the dynamics of necking and fragmentation – I. Real-time and post-mortem observations in Al 6061-O*, Int. J. Fract., **142**, 183–217, 2006.
26. H. ZHANG, K. RAVI-CHANDAR, *On the dynamics of necking and fragmentation – II. Effect of material properties, geometrical constraints and absolute size*, Int. J. Fract., **150**, 3–36, 2008.
27. S. MERCIER, A. MOLINARI, *Analysis of multiple necking in rings under rapid radial expansion*, Int. J. Impact. Eng., **4**, 403–419, 2004.
28. A. RUSINEK, R. ZAERA, *Finite element simulation of steel ring fragmentation under radial expansion*, Int. J. Impact. Eng., **34**, 799–822, 2007.
29. U. F. KOCKS, A. S. ARGON, M. F. ASHBY, *Thermodynamics and kinetics of slip*, [in:] Progress in Materials Science, vol. 19, Chalmers B., Christian J.W., Massalski T.B. [Eds.], Pergamon Press, Oxford, 1975.
30. F. J. ZERILLI, R. W. ARMSTRONG, *Dislocation-mechanics-based constitutive relations for material dynamics calculations*, J. Appl. Phys., **61**, 1816–1825, 1987.
31. S. NEMAT-NASSER, Y. LI, *Flow stress of FCC polycrystals with application to OFHC Copper*, Acta Mater., **46**, 565–577, 1998.
32. A. RUSINEK, J. R. KLEPACZKO, *Shear testing of sheet steel at wide range of strain rates and a constitutive relation with strain-rate and temperature dependence of the flow stress*, Int. J. Plasticity, **17**, 87–115, 2001.
33. S. NEMAT-NASSER, W. G. GUO, *Thermomechanical response of DH-36 structural steel over a wide range of strain rates and temperatures*, Mech. Mat., **35**, 1023–1047, 2003.
34. G. Z. VOYIADJIS, F. H. ABED, *Microstructural based models for bcc and fcc metals with temperature and strain rate dependency*, Mechanics of Materials, **37**, 355–378, 2005.
35. F. H. ABED, G. Z. VOYIADJIS, *Plastic deformation modeling of AL-6XN stainless steel at low and high strain rates and temperatures using a combination of bcc and fcc mechanisms of metals*, Int. J. Plasticity, **21**, 1618–1639, 2005.
36. G. Z. VOYIADJIS, A. H. ALMASRI, *A physically based constitutive model for fcc metals with applications to dynamic hardness*, Mech. Mater., **40**, 549–563, 2008.
37. A. RUSINEK, J. A. RODRÍGUEZ-MARTÍNEZ, R. ZAERA, J. R. KLEPACZKO, A. ARIAS, C. SAUVELET, *Experimental and numerical analysis of failure process of mild steel sheets subjected to perpendicular impact by hemispherical projectiles*, Int. J. Impact. Eng., **36**, 565–587, 2009.
38. A. RUSINEK, J. A. RODRÍGUEZ-MARTÍNEZ, A. ARIAS, *A thermo-viscoplastic constitutive model for FCC metals with application to OFHC copper*, Int. J. Mech. Sci., **52**, 120–135, 2010.
39. M. C. CAI, L. S. NIU, X. F. MA, H. J. SHI, *A constitutive description of the strain rate and temperature effects on the mechanical behavior of materials*, Mech. Mat., **42**, 774–781, 2010.

40. C. Y. GAO, L. C. ZHANG, *A constitutive model for dynamic plasticity of FCC metals*, *Materials Science and Engineering A.*, **527**, 3138–3143, 2010.
41. A. SEEGER, *The mechanism of glide and work-hardening in face centered cubic and hexagonal close-packed metal*, [in:] *Dislocations and Mechanical Properties of Crystals*, J. Wiley, New York, 1957.
42. U. F. KOCKS, *Realistic constitutive relations for metal plasticity*, *Mat. Sci. and Eng. A.*, **317**, 181–187, 2001.
43. J. A. RODRÍGUEZ-MARTÍNEZ, A. RUSINEK, J. R. KLEPACZKO, *Constitutive relation for steels approximating quasi-static and intermediate strain rates at large deformations*, *Mech. Res. Com.*, **4**, 419–427, 2009.
44. J. R. KLEPACZKO, *A general approach to rate sensitivity and constitutive modeling of FCC and BCC metals*, [in:] *Impact: Effects of Fast Transient Loadings*, Rotterdam, 3–35, 1998.
45. A. RUSINEK, J. A. RODRÍGUEZ-MARTÍNEZ, J. R. KLEPACZKO, R. B. PECHERSKI, *Analysis of thermo-visco-plastic behaviour of six high strength steels*, *J. Mater. Des.*, **30**, 1748–1761, 2009.
46. P. S. FOLLANSBEE, U. F. KOCKS, *A constitutive description of the deformation of copper based on the use of the mechanical threshold stress as an internal state variable*, *Acta Metall.*, **1**, 81–93, 1988.
47. J. R. KLEPACZKO, *Thermally activated flow and strain rate history effects for some polycrystalline f.c.c. metals*, *Materials Science and Engineering*, **18**, 121–135, 1975.
48. J. R. KLEPACZKO, B. REZAIG, *A numerical study of adiabatic shear banding in mild steel by dislocation mechanics based constitutive relations*, *Mechanics of Materials*, **24**, 125–139, 1996.
49. R. KAPOOR, S. NEMAT-NASSER, *Comparison between high strain-rate and low strain-rate deformation of tantalum*, *Metall. Mater. Trans.*, **31A**, 815–823, 1999.
50. S. NEMAT-NASSER, W. G. GUO, D. P. KIHIL, *Thermomechanical response of AL-6XN stainless steel over a wide range of strain rates and temperatures*, *J. Mech. Phys. Solids*, **49**, 1823–1846, 2001.
51. A. RUSINEK, J. A. RODRIGUEZ-MARTINEZ, R. PESCI, J. CAPELLE, *Experimental characterisation and modelling of the thermo-viscoplastic behaviour of steel AISI 304 within wide ranges of strain rate at room temperature*, *Journal of Theoretical and Applied Mechanics*, 2010 [in press].
52. O. OUSSOUADDI, J. R. KLEPACZKO, *An analysis of transition from isothermal to adiabatic deformation in the case of a tube under torsion* [in French], *Proceedings Conf. DYMAT 91*, *Journal de Physique IV 1991*, Coll. C3 (Suppl. III), C3–323.
53. A. RUSINEK, R. ZAERA, J. R. KLEPACZKO, *Constitutive relations in 3-D for a wide range of strain rates and temperatures – application to mild steels*, *Int. J. Solids Struct.*, **44**, 5611–5634, 2007.
54. P. S. FOLLANSBEE, *High-strain-rate deformation of FCC metals and alloys*, [in:] *Metalurgical applications of shock-wave and high-strain-rate phenomena*, pp. 451–479, 1986.
55. J. A. ZUKAS, D. R. SCHEFFLER, *Practical aspects of numerical simulations of dynamic events: effects of meshing*, *Int. J. Impact Eng.*, 925–945, 2000.

56. M. LARSON, A. NEEDLEMEN, V. TVERGAARD, B. STORAKERS, *Instability and failure of internally pressurized ductile metal cylinders*, Internal report, Division of Engineering, Brown University, Providence, June 1981.
57. J. B. HAN, V. TVERGAARD, *Effect of inertia on the necking behaviour of ring specimens under rapid axial expansion*, Eur. J. Mech. A/Solids, **14**, 287–307, 1995.
58. N. J. SORENSEN, L. B. FREUND, *Unstable neck formation in a ductile ring subjected to impulsive radial loading*, Int. J. Solids Struct., **37**, 2265–83, 2000.
59. G. Z. VOYIADJIS, F. H. ABED, *A coupled temperature and strain rate dependent yield function for dynamic deformations of bcc metals*, International Journal of Plasticity, **22**, 1398–1431, 2006.
60. J. A. NEMES, J. EFTIS, *Constitutive modelling on the dynamic fracture of smooth tensile bars*, International Journal of Plasticity, **9**, 243–270, 1993.
61. R. ZAERA, J. FERNÁNDEZ-SÁEZ, *An implicit consistent algorithm for the integration of thermoviscoplastic constitutive equations in adiabatic conditions and finite deformations*, Int. J. Solids Struct., **43**, 1594–1612, 2006.
62. N. TRIANTAFYLIDIS, J. R. WALDENMYER, *Onset of necking in electro-magnetically formed rings*, J. Mech. Phys. Solids, **52**, 2127–2148, 2004.

*Received May 11, 2011.*

---